

## Supplementary Materials

### Experimental

#### *Synthesis of electrocatalysts*

$\text{SrSc}_x\text{Nb}_y\text{Co}_{1-x-y}\text{O}_{3-\delta}$  (SSNC) was synthesized via a solid-state reaction using  $\text{SrCO}_3$ ,  $\text{Sc}_2\text{O}_3$ ,  $\text{Nb}_2\text{O}_5$  and  $\text{Co}_3\text{O}_4$  (Sigma-Aldrich) as the raw materials (for the metal sources). The raw materials were weighed and mixed inside a planetary mill (Fritsch, Pulverisette 5) using ethanol media at a rotation rate of 400 rpm for 2 hours. After drying, the primary powders were calcined at 1200 °C in air for 40 hours, and then ground in an agate mortar and calcined at 1250 °C for 20 hours to form the perovskite oxides.

Other perovskites, including BSCF, SCF, LSCF, LSC, LSF, and LN, were synthesized via an ethylenediaminetetraacetic acid (EDTA)/citrate complexing process. Take BSCF perovskite oxide as an example.  $\text{Ba}(\text{NO}_3)_2$ ,  $\text{Sr}(\text{NO}_3)_2$ ,  $\text{Fe}(\text{NO}_3)_3 \cdot 9\text{H}_2\text{O}$  and  $\text{Co}(\text{NO}_3)_2 \cdot 6\text{H}_2\text{O}$  (Sigma-Aldrich) were used as the raw materials (for metal sources). Stoichiometric amounts of these metal nitrates were mixed in de-ionized water and heated to 80 °C. EDTA (99.9%, Sigma-Aldrich) and anhydrous citric acid (99.5%, Fluka) were then added as the complexing agents. The molar ratio of total metal nitrates, EDTA and citric acid in the solution was 1:1:2. To ensure complete complexation, the solution pH was adjusted to 8 by adding aqueous  $\text{NH}_3$  solution (25%), resulting in a violet transparent aqueous solution. After evaporation of water at 120 °C, a dark purple gel was recovered. The gel was pre-treated in the furnace at 250 °C for 8 hours to form a solid precursor. The solid precursor was then ground into powder and calcined at 800-1050 °C for 5 hours in air. The calcination temperature for each perovskite is listed as below. The BSCF was also synthesized by solid state reaction with similar process as SSNC at 1050 °C for 5 hours in air. The synthetic conditions for each sample are listed as below.

Sample names	Synthesis methods	Calcination temperatures ( °C)
BSCF1	EDTA-citrate	900
BSCF2	EDTA-citrate	1000
BSCF3	solid state reaction	1050
SCF	EDTA-citrate	900
LSCF	EDTA-citrate	800
LSC	EDTA-citrate	800
LN	EDTA-citrate	800
SSNC1	solid state reaction	1250
SSNC2	solid state reaction	1250
SSNC3	solid state reaction	1250
SSNC4	solid state reaction	1250
SSNC5	solid state reaction	1250
SSNC6	solid state reaction	1250
SSNC7	solid state reaction	1250
SSNC8	solid state reaction	1250

All the synthesized powders were ground by hand to obtain the samples for OER test without any mechanical milling to crash the samples.

### ***Sample Characterizations***

Powder X-ray diffraction (XRD) analysis was utilized to identify the crystallite structures of synthesized powders at room temperature and was performed on a Bruker D8 Advance instrument using monochromator-filtered Cu-K $\alpha$  radiation at 40 kV. The data were collected in a step-scan mode in the range of 15-90 ° with intervals of 0.01 ° at a scanning rate of 2° min<sup>-1</sup>. The chemical state of O was analysed by XPS (Kratos Axis ULTRA). The samples for XPS analysis were obtained immediately after the synthesis to avoid the formation of the carbonates on the surface of the perovskites.

The water desorption properties of the perovskites was investigated by both thermogravimetric analysis (TGA) and a Bel-Catal connected with a mass spectrometer (Japan Bel Inc.,). In both cases, approximately 100 mg as-synthesized perovskite powder was loaded into a ZrO<sub>2</sub> crucible and then the crucible was put in a tubular reactor for the test. The experiments were carried out from 25 to 350 °C at a heating-rate of 10 °C min<sup>-1</sup> under Ar atmosphere.

Transmission electron microscopy (TEM) was performed at 200 kV on a field-emission instrument of type JEOL JEM-2100F. The morphology of the material was studied by FESEM (JEOL 7001). The Brunauer-Emmett-Teller (BET) surface area of the powders was measured using N<sub>2</sub>-adsorption measurements on a Micromeritics TriStar II 3020, after degassing the samples for 24 hours at 190 °C prior to the test.

### ***Electrochemical characterization***

For the purpose of lifting electronic conductivity restrictions within the thin film electrodes, the as-synthesised sample electrocatalysts were mixed with as received carbon (Super C65) from TIMCAL C'NERGY at mass ratio of 1:1. The electrocatalyst suspension was prepared by sonication of electrocatalyst (10 mg), carbon (10 mg), ethanol (1 mL) and Nafion solution (5 wt%, 100 µL) for 30 min. An aliquot of 5 µL of mixture suspension was drop-casted onto a glassy carbon disk electrode (4 mm diameter, 0.126 cm<sup>2</sup> area) and left under a glass jar for drying for three hours. The mass loading of perovskite oxide is 0.36 mg cm<sub>disk</sub><sup>-2</sup>.

Voltammetric experiments were performed with a Biologic VMP2/Z multichannel potentiostat. Rotating disk electrode (RDE) voltammograms were obtained in an O<sub>2</sub>(99.999%) saturated 0.1 M KOH solution at 10 mV s<sup>-1</sup> at room temperature using a platinum wire counter electrode and a Ag|AgCl (3M NaCl) reference electrode, which

was calibrated with respect to reversible hydrogen electrode (RHE). The calibration was performed in the high purity hydrogen saturated electrolyte with a Pt wire as the working electrode. CVs were run at a scan rate of  $1 \text{ mV s}^{-1}$ , and the average of the two potentials at which the current crossed zero was taken to be the thermodynamic potential for the hydrogen electrode reactions. All the potentials in this study are iR-corrected potentials to compensate for the effect of solution resistance, which were calculated by the following equation:

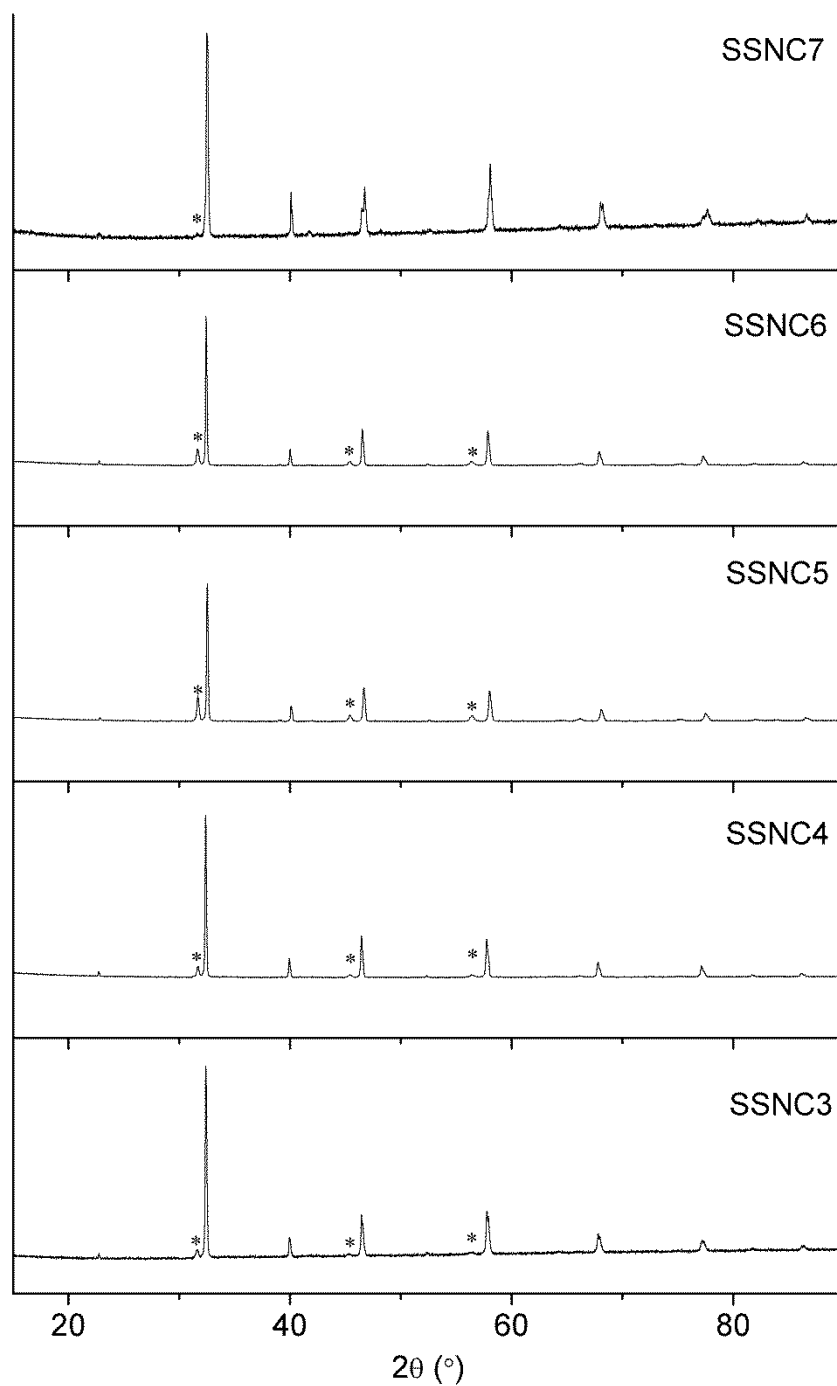
$$E_{RHE(iR\text{-corrected})} = E_{Ag|AgCl} + 0.937 - iR \quad (1)$$

Where  $i$  is the current and  $R$  is the uncompensated ohmic electrolyte resistance measured via high frequency ac impedance in  $O_2$ -saturated 0.1 M KOH. For the stability test, chronoamperometry data were collected at a potential of 0.7 V vs Ag|AgCl (3M NaCl) and the CV tests were run at a scan rate of  $50 \text{ mV s}^{-1}$ .

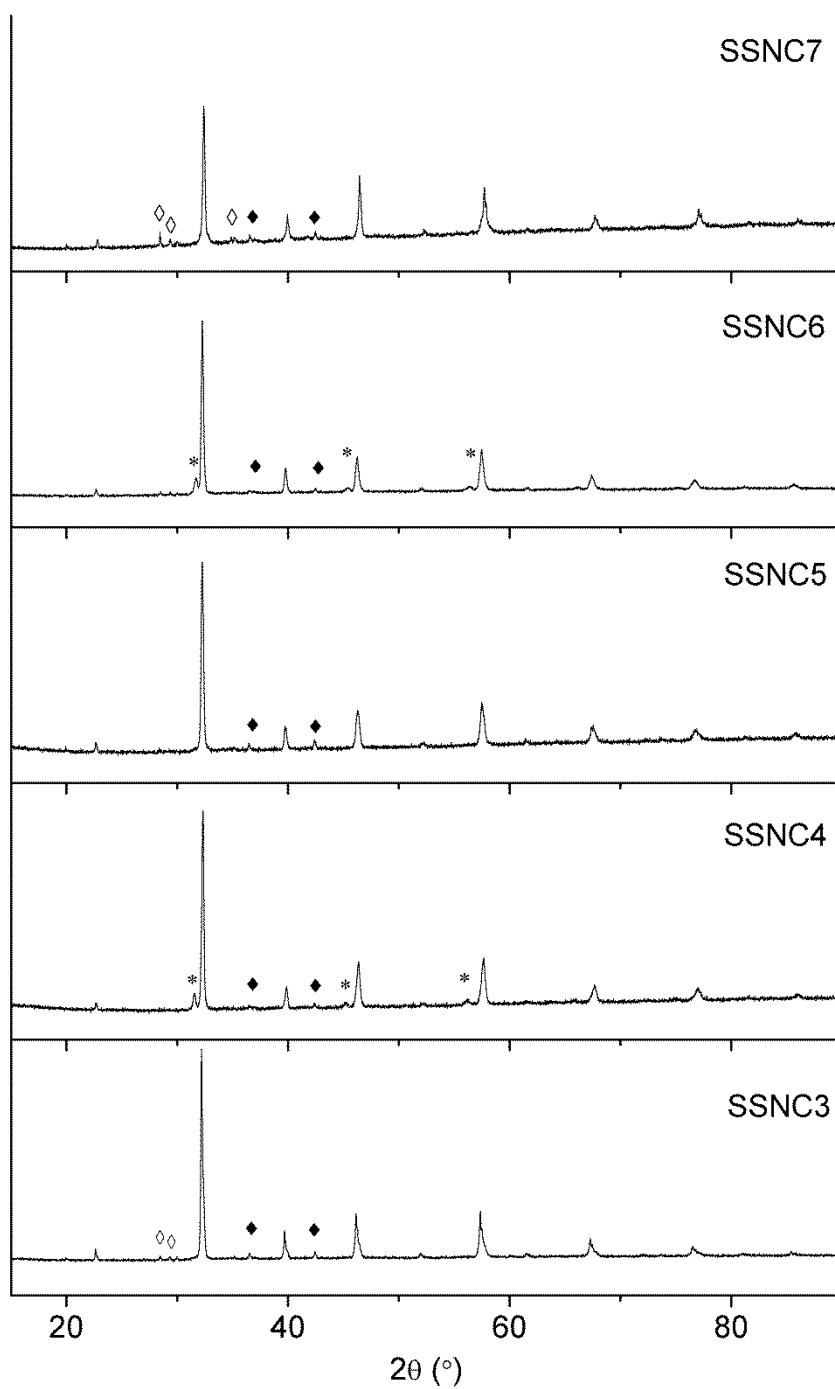
### ***Theoretical method and computational details***

The first-principles calculations were performed with the Vienna *ab initio* simulation package (VASP) [S1, S2] using density-functional theory (DFT). The ion-electron interactions are treated using projector-augmented-wave potentials [S3]. A generalized gradient approximation (GGA) in the form of Perdew-Burke-Ernzerhof is adopted to describe the electron-electron interactions [S4]. The GGA+U calculations are performed with the simplified spherically averaged approach, where the  $U_{\text{eff}}$  ( $U_{\text{eff}}=U - J$ ) is applied to  $d$  electrons. The electron wave functions are expanded using the plane waves with the energy cutoff of 520 eV. The Kohn-Sham equation is solved self-consistently with the convergence of  $10^{-5}$ . A four layer slab with a  $(2 \times 2)$  unit cells separated by a more than 15 Å of vacuum were employed to represent a surface (Fig. S10). The two topmost layers were allowed to fully relax, while the other layers were fixed to their optimized bulk position. The Brillouin zone is integrated with symmetry reduced  $(4 \times 4 \times 1)$  Monkhorst-Pack mesh. Structural optimizations are carried out using a conjugated gradient (CG) method until the remaining force on each atom is lower than  $0.01 \text{ eV/\AA}$ . The overpotentials  $\eta^{\text{OER}}$  were calculated from four electron reaction paths using the standard hydrogen electrode (SHE) model [S5].

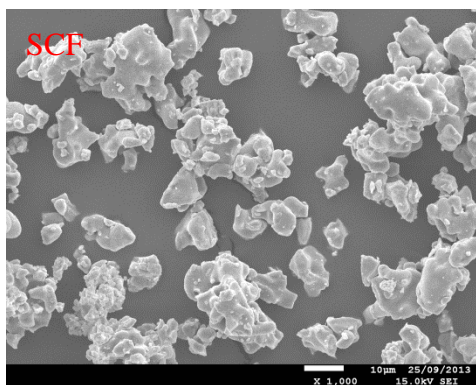
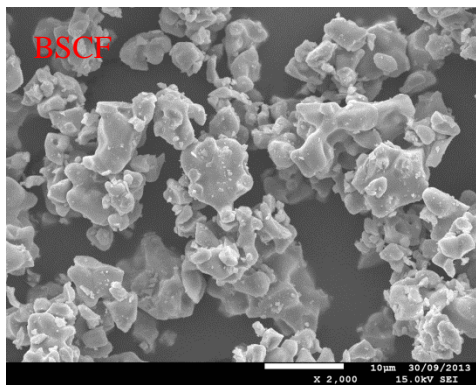
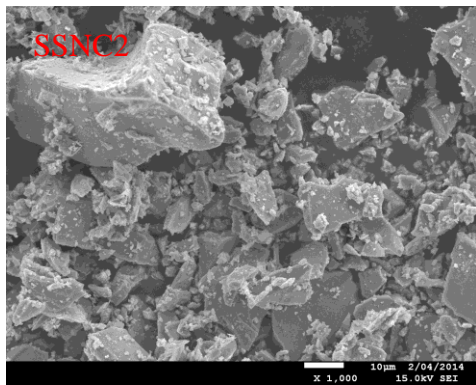
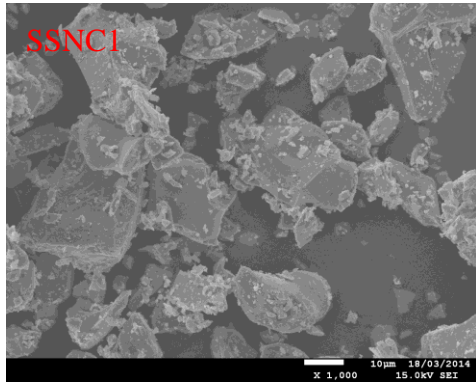




**Figure S2** X-ray diffraction profiles of SSNC3-7 calcined at 1250 °C. \* notes the brown-millerite phase.



**Figure S3** X-ray diffraction profiles of SSNC3-7 calcined at 1300 °C. \* : the brown-millerite phase, ◆: CoO, ◇: unknown phase.



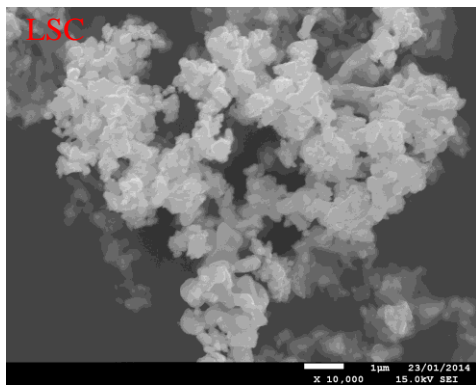
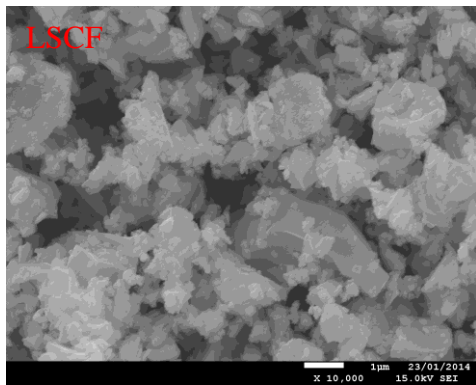
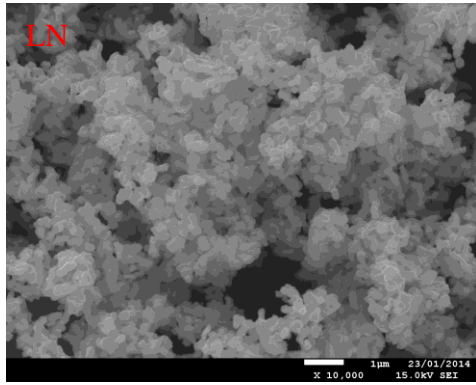


**Figure S4** SEM images of SSNC1, SSNC2, BSCF, SCF, LN, LSCF and LSC.

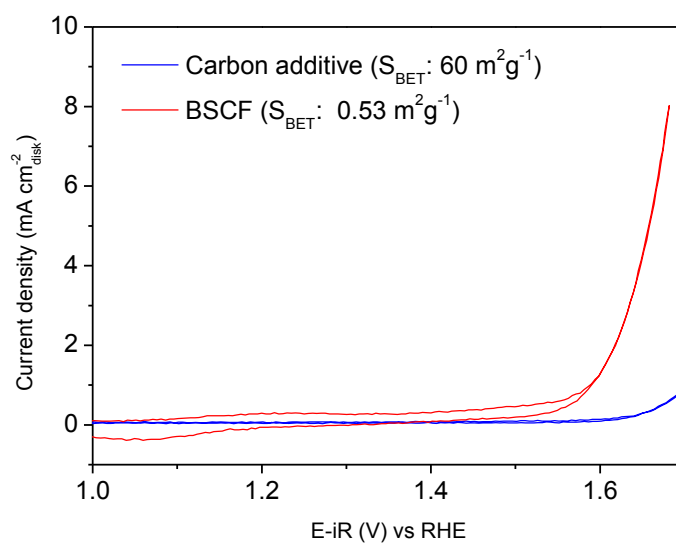


**Figure S5** The OER activity of the carbon black ( $0.36 \text{ mg cm}_{\text{disk}}^{-2}$ ) that used as the conductive additive in the present study. The OER activity of BSCF was shown for comparison.

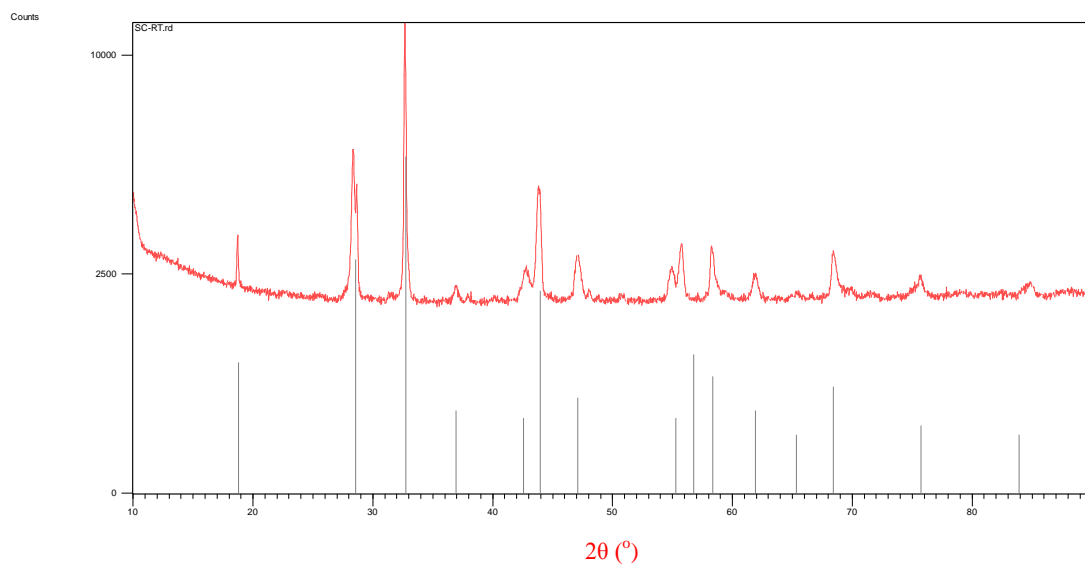


**Figure S6** XRD pattern of as-synthesized  $\text{SrCoO}_{3-\delta}$ . The vertical bars are indexed as  $\text{SrCoO}_{2.5}$  in brownmillerite structure. The phase structure of the as-synthesized  $\text{SrCoO}_{3-\delta}$  can be indexed to brownmillerite with  $\delta$  approaching 0.5.

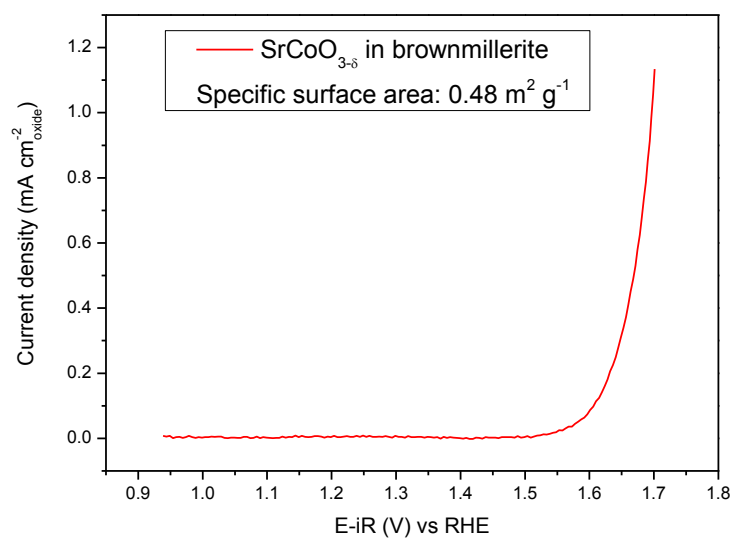


**Figure S7** LSV *iR*-corrected polarization curves of SrCoO<sub>3-δ</sub> in brownmillerite structure.

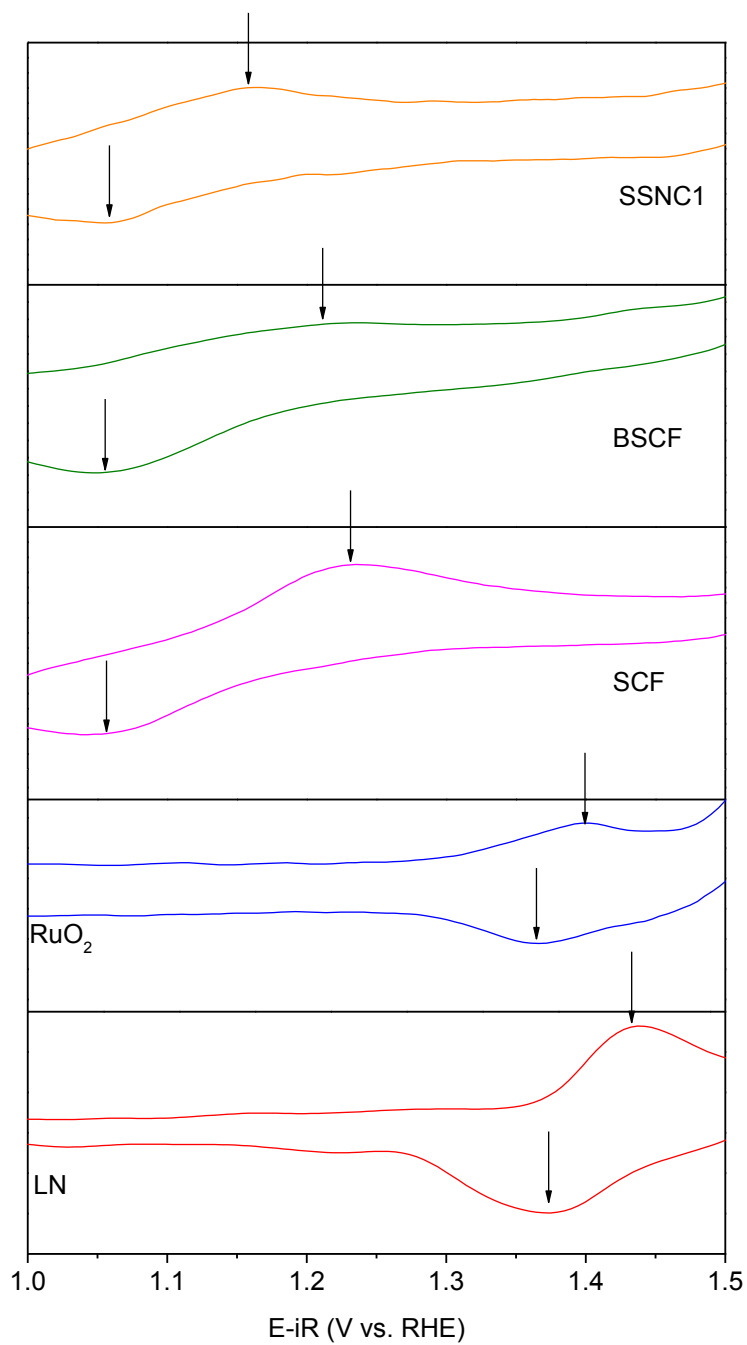


**Figure S8** Cyclic voltammograms of SSNC1, BSCF, SCF, RuO<sub>2</sub> and LN electrocatalysts in 0.1M KOH at scan rate of 5 mV s<sup>-1</sup>. The arrows note the redox couple peaks for the electrocatalysts in cyclic voltammogram test.

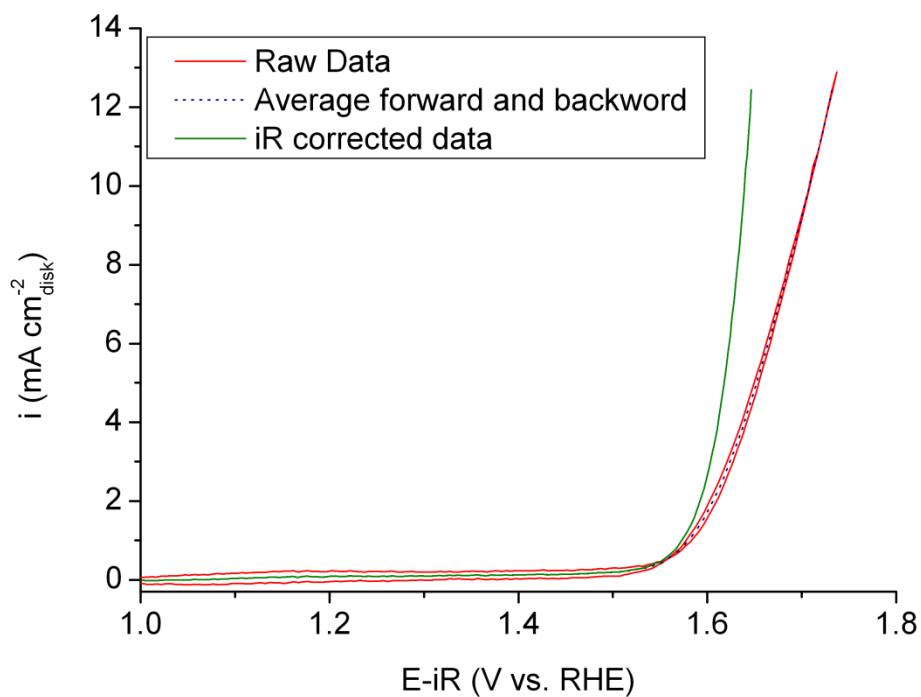


**Figure S9** Ohmic and capacitive corrections of the as-measured OER activity of example perovskite oxide catalyst (the method is described in Ref [S5]). The as-measured OER activity of the thin-film SSNC1 electrocatalyst (“raw”, solid red line) is capacity-corrected by taking an average of forward and backward (positive and negative-going) scans. The capacity-corrected OER current (short-dash blue line) is then ohmically corrected with the measured ionic resistance ( $\approx 55 \Omega$ ) to yield the final electrode OER activity (green line).

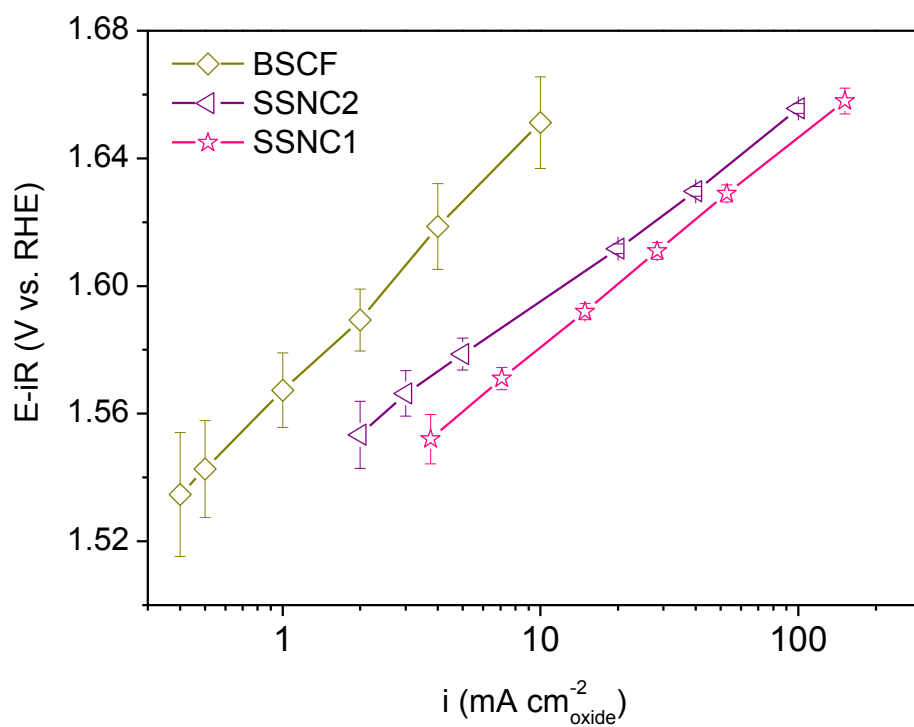


**Figure S10** Intrinsic OER activities of SSNC1, SSNC2 and BSCF normalized by the true oxide surface area, which were obtained from averaging currents in the forward and backward scans of the second cycle and subtracting the ohmic losses. All the samples were measured at least three times to obtain the data corrected with the standard deviations

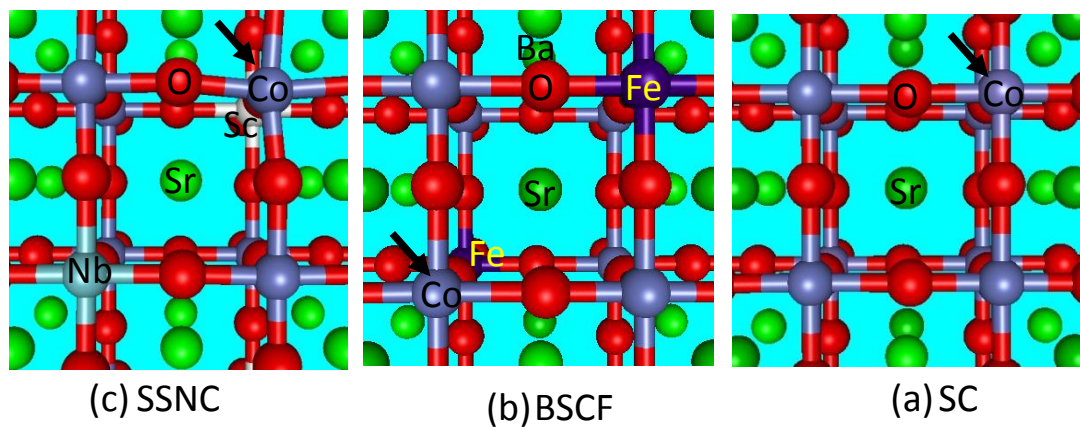


**Figure S11** Atomic structures (top view) of the (100) surface of (a) SSNC, (b) BSCF, and (c) SC. The active Co atoms are indicated by the arrows.

## Tables

**Table S1.** The crystal structure determined by XRD and specific surface area of the samples were determined from nitrogen Brunauer, Emmett, and Teller (BET) area measurements

Sample	Crystal structure	Specific surface area ( $\text{m}^2 \text{g}^{-1}$ )	Loading of the electrocatalysts ( $\text{mg cm}_{\text{disk}}^{-2}$ )
$\text{SrSc}_{0.025}\text{Nb}_{0.025}\text{Co}_{0.95}\text{O}_{3-\delta}$ (SSNC1)	P1121/a	0.1	0.36
$\text{SrSc}_{0.175}\text{Nb}_{0.025}\text{Co}_{0.8}\text{O}_{3-\delta}$ (SSNC2)	Pm-3m	0.14	0.36
$\text{SrSc}_{0.025}\text{Nb}_{0.075}\text{Co}_{0.9}\text{O}_{3-\delta}$ (SSNC3)	P1121/a, impurity: brown-millerite phase	0.13	0.36
$\text{SrSc}_{0.15}\text{Nb}_{0.05}\text{Co}_{0.8}\text{O}_{3-\delta}$ (SSNC4)	Pm-3m, impurity: brown-millerite phase	0.18	0.36
$\text{SrSc}_{0.125}\text{Nb}_{0.075}\text{Co}_{0.8}\text{O}_{3-\delta}$ (SSNC5)	Pm-3m, impurity: brown-millerite phase	0.17	0.36
$\text{SrSc}_{0.05}\text{Nb}_{0.05}\text{Co}_{0.9}\text{O}_{3-\delta}$ (SSNC6)	P1121/a, impurity: brown-millerite phase	0.12	0.36
$\text{SrSc}_{0.1}\text{Nb}_{0.05}\text{Co}_{0.85}\text{O}_{3-\delta}$ (SSNC7)	Pm-3m, impurity: brown-millerite phase	0.13	0.36
$\text{SrSc}_{0.1}\text{Nb}_{0.1}\text{Co}_{0.8}\text{O}_{3-\delta}$ (SSNC8)	Pm-3m, impurity: brown-millerite phase	0.15	0.36
$\text{La}_{0.6}\text{Sr}_{0.4}\text{Co}_{0.2}\text{Fe}_{0.8}\text{O}_{3-\delta}$ (LSCF)	R-3c	5.1	0.36
$\text{La}_{0.6}\text{Sr}_{0.4}\text{CoO}_{3-\delta}$ (LSC)	R-3m	2.9	0.36
$\text{LaNiO}_{3-\delta}$ (LN)	R-3c	3.1	0.36
BSCF	Pm-3m	0.53	0.36
BSCF1	Pm-3m	0.33	0.36
BSCF2	Pm-3m	0.15	0.36
$\text{SrCo}_{0.8}\text{Fe}_{0.2}\text{O}_{3-\delta}$ (SCF)	Pm-3m	0.68	0.36
$\text{RuO}_2$	P42/mnm	4.6	0.36
$\text{IrO}_2$	P42/mnm	5.4	0.36

**Table S2.** O1s XPS peak deconvolution results for SSNC1, SSNC2, BSCF and LN

Electrocatalysts	H <sub>2</sub> O	-OH	O <sub>2</sub> <sup>2-</sup> + O <sup>-</sup>	O <sup>2-</sup>
<b>SSNC1</b>	8.78	65.27	10.28	15.67
<b>SSNC2</b>	8.94	65.15	2.74	23.17
<b>BSCF</b>	9.44	33.01	34.56	22.99
<b>LN</b>	11.14	29.84	24.60	34.43

**Table S3** Calculated free energy  $\Delta G_{1-4}$  and overpotential  $\eta^{OER}$  for SrCoO<sub>3</sub>, SSNC and BSCF perovskite electrocatalysts.

	SrCoO <sub>3</sub>	SSNC	BSCF
$\Delta G_1^0$ (eV)	1.439	1.736	1.857
$\Delta G_2^0$ (eV)	1.515	1.342	1.340
$\Delta G_3^0$ (eV)	1.565	1.789	1.866
$\Delta G_4^0$ (eV)	0.840	0.494	0.298
$\eta^{OER}$ (V)	0.335	0.559	0.636

The following four electron reaction paths (Equations (1)–(4)) were considered as the pathway for water oxidation [S6].



$$\Delta G_1 = \Delta G_{\text{HO}^*} - \Delta G_{\text{H}_2\text{O}(\text{l})} - eU + k_b T \ln a_{\text{H}^+}$$



$$\Delta G_2 = \Delta G_{\text{O}^*} - \Delta G_{\text{HO}^*} - eU + k_b T \ln a_{\text{H}^+}$$



$$\Delta G_3 = \Delta G_{\text{HOO}^*} - \Delta G_{\text{O}^*} - eU + k_b T \ln a_{\text{H}^+}$$



$$\Delta G_4 = \Delta G_{\text{O}_2} - \Delta G_{\text{HOO}^*} - eU + k_b T \ln a_{\text{H}^+}$$

The theoretical overpotential ( $\eta^{OER}$ ), which is independent of pH, at standard conditions is then given by Equation (5):

$$\eta^{OER} = G^{OER}/e - 1.23V \quad (5)$$

$$G^{OER} = \max[\Delta G_1^0, \Delta G_2^0, \Delta G_3^0, \Delta G_4^0] \quad (6)$$

For which  $\Delta G_{1-4}^0$  is  $\Delta G_{1-4}$  at  $U=0$  (pH=0 and T=298.15 K).

The overpotential difference between SSNC and BSCF is

$$\Delta \eta^{OER} = 0.636 - 0.559 = 0.077V.$$

## References

- [S1]G. Kresse, J. Hafner, Ab initio molecular dynamics for open-shell transition metals. *Phys. Rev.* **B48**, 13115 (1993).
- [S2]G. Kresse, J. Furthmuller, Efficient iterative schemes for ab initio total-energy calculations using a plane-wave basis set. *Phys. Rev. B: Condensed Matter* **54**, 11169-11186 (1996).
- [S3]G. Kresse, D. Joubert, From ultrasoft pseudopotentials to the projector augmented-wave method. *Phys. Rev. B* **59**, 1758-1775 (1999).
- [S4]J. P. Perdew, K. Burke, M. Ernzerhof, Generalized gradient approximation made simple. *Phys. Rev. Lett.* **77**, 3865-3868 (1996).
- [S5]Suntivich, J., May, K. J., Gasteiger, H. A., Goodenough, J. B. & Shao-Horn, Y. A perovskite oxide optimized for oxygen evolution catalysis from molecular orbital

principles. *Science* **334**, 1383-1385 (2011).  
[S6]I. C. Man et al., Universality in Oxygen Evolution Electrocatalysis on Oxide Surfaces, *ChemCatChem* **3**, 1159-1165 (2011).